

Universidad de La Laguna

FACULTAD DE CIENCIAS: SECCIÓN DE FÍSICA

TRABAJO DE FIN DE GRADO

An introduction to global optimization of atomic
clusters

José María Ramos Fernández

Supervisado por: Dr. Javier Hernández Rojas

Julio 2021

Resumen

Los problemas de optimización global aparecen en diferentes disciplinas y presentan una amplia gama de aplicaciones prácticas, por lo que el estudio de estos es un campo de creciente interés en la actualidad. Este trabajo se centra en los problemas de optimización global que aparecen en la física de agregados atómicos. Se lleva a cabo un breve recopilatorio sobre métodos de optimización global que han conseguido buenos resultados en los últimos años y se introduce el marco teórico necesario para el estudio de los agregados atómicos en este contexto. Asimismo, se implementa uno de los métodos de la bibliografía, el Basin-Hopping (BH), para el estudio de agregados modelizados por los potenciales de Lennard-Jones (LJ) y de Morse (M) que contengan hasta 50 átomos. Con este algoritmo se han podido encontrar, utilizando búsquedas no guiadas, todos los mínimos de energía y sus estructuras asociadas para los dos tipos diferentes de agregados estudiados (LJ y M).

Agradecimientos

Gracias a mi tutor, Javier Hernández Rojas, por resolver todas mis dudas y permitir que este trabajo salga adelante a pesar de los inconvenientes que fueron surgiendo.

Gracias a Luis Pedro, aún no sé quién eres, pero siempre consigues sacarme una sonrisa.

Gracias a todos los compañeros de C.M. y a Paola, Ikeya y Milva; sin duda han sido 4 años de duro trabajo, pero han estado edulcorados por su siempre estupenda compañía que me ha ayudado a crecer. Igualmente, gracias por muchas veces ser luz donde uno solo encuentra oscuridad. Se les quiere.

Gracias también a mi familia, especialmente a mis padres, que siempre me han apoyado y apoyan en todo lo que persigo. Y a mi abuela, por encender una velita en su casa los días de examen. También a mis hermanos, por ellos sigo siendo un niño durante algo más de tiempo.

Gracias a Irene, por aguantarme las mil frases con el “¿cómo lo ves?” y, por supuesto, gracias a Aitor por literalmente salvar este trabajo.

Contents

Resumen	I
Agradecimientos	II
List of Figures	IV
1 Introduction	1
2 The global optimization problem (GOP) and the methods for its resolution	4
The general GOP	4
The case study: atomic clusters	6
3 Interatomic potentials	7
The Born-Oppenheimer approximation	7
Interatomic potentials	10
The Lennard-Jones (LJ) potential	10
The Morse (M) potential	12
4 The implemented method: Basin-Hopping	15
The fundamentals of the algorithm	15
Algorithm and code efficiency	18
5 Results and analysis	20
The results for the energies	20
Cluster stability and geometry	22
Second-order difference of cluster energies	23
Geometry of the clusters	24
Icosahedral structures	25
The 38-atom cluster	26
6 Conclusions	28
References	i
Appendix A: Derivatives of the Lennard-Jones and Morse potentials.	A1
Appendix B: All the structures obtained for the Lennard-Jones potential excluding the 2 particle case.	B1

List of Figures

2.1	Surface plot of the function $f(x, y) = [\sin(xy) + \sin(3y - 5x) + \sin(x^2 - 4y) - 2]^2$ within the domain $D = \{-3 \leq x \leq 3; -2 \leq y \leq 5\}$ to illustrate how complex the GOP can become in higher dimensions and bigger domains.	5
3.1	LJ potential for a 2 particle system.	11
3.2	M potential for different values of the variable parameter ρ_0	12
3.3	“Phase diagram” showing how lowest-energy structures change according to the values of N and ρ_0 . PT means polytetrahedral structures and L structures associated with low ρ_0 . Extracted from [10].	13
3.4	A representation of both the M and the LJ potentials.	14
4.1	Flowchart for the BH method.	16
4.2	Scheme of the functioning of the BH method in a simple one dimensional case.	17
5.1	Energy per particle obtained for each cluster using LJ and Morse potentials.	21
5.2	Differences between the energies per particle obtained for each cluster with the LJ and M potentials.	21
5.3	Representation of the mean number of necessary jumps for achieving the global minimum for each of the clusters size.	22
5.4	A representation of the second-order energy differences $\Delta_2 E(N)$ for each cluster size and both potentials, LJ and M.	23
5.5	Atomic positions for the two possible overlayers of the icosahedron, anti-Mackay (left) and Mackay (right). These are shown for a single face of the icosahedron. Extracted from [15].	24
5.6	Structures obtained for the so called “magic numbers”, clusters with a certain number of atoms which give rise to a particularly high stability. .	25
5.7	The global minimum structure (left) and the second lowest energy structures (right) found for the LJ_{38} cluster.	27
A1	Representation of the derivatives of both potentials, LJ and M, for a two particle system.	A1

1 Introduction

Resumen

La optimización global es un campo de investigación bastante activo en la actualidad debido a sus aplicaciones prácticas que pueden implicar importantes beneficios económicos. Aunque sus aplicaciones abarcan un amplio número de áreas, este trabajo se centra en la física de agregados atómicos. Un agregado atómico es un conjunto de átomos o iones que forma una estructura debido a fuerzas similares a las que mantienen unidos a los átomos o iones que conforman la materia macroscópica.

Este trabajo pretende servir como introducción a la optimización global en agregados atómicos. Con esta intención, se comentan distintos métodos de optimización global disponibles en la actualidad, se establece el marco teórico en el que estudios como este pueden tener lugar y se plantea un caso práctico que se centra en la obtención de los mínimos de energía y las estructuras asociadas a estos para agregados de hasta 50 átomos modelizados por dos potenciales: LJ, que sirve como buen modelo para agregados de gases ideales, y M, muy utilizado para el estudio de moléculas diatómicas. Para llevar a cabo la búsqueda de estas energías mínimas, que dado el caso coincide con buscar el mínimo absoluto de los potenciales utilizados, se implementa un método de optimización basado en la estrategia de basin-hopping utilizando el lenguaje de programación Python.

Global optimization is a field of current active investigation due to its applications to different practical cases that, eventually, will or can lead to important economic advantages. Complex optimization problems appear in many different fields, ranging from physics to economics. A typical optimization problem, with obvious economic impact, is given by the traveling salesman problem, which, given a set of cities and costs, strives to find the route that minimizes the costs. In other fields, the optimization problem plays an important role for different issues that include from protein structure prediction to the design of microprocessor circuitry [1]. Nevertheless, this work is focused on global optimization in the context of cluster science.

Clusters are aggregates of atoms or ions that adhere together under forces like those that bind the atoms or ions of bulk matter. Clusters are prepared in such way that they remain as tiny particles at least during the realization of an experiment. The forces that maintain the atoms together to form clusters are van der Waals forces, ionic forces, covalent and metallic bonds. In spite of the similarity of these forces with the ones that bind macroscopic matter, there is a very interesting thing about clusters, that is that

their properties are different from those of the corresponding macroscopic material. As an example, a cluster of 20-30 atoms typically has a melting point far lower than the one of the corresponding bulk matter. In some cases, electrical properties of clusters also differ from those of the bulk matter. This raises the question on how the properties of clusters evolve towards the properties of bulk matter as the number of constituents increases.[2].

This work is focused on the characterization of the structures associated to the ground-state energy level of clusters. For this purpose, the interaction between atoms needs to be characterized by some means. In the conditions of this study, the Born-Oppenheimer approximation can be applied and so the nuclear and electronic motion can be separated. Within this context, the concept of potential energy (hyper)surface (PES) appears, which is a function that describes the interaction between all the atoms that make up the cluster. In view of this, developing potential energy functions that describe accurately the interaction between the parts of the system is a subject of current intense investigation [1].

Nowadays, there are already a great amount of potentials which can be used for modelling clusters. As these potential energy functions describe the interaction of the atoms in the cluster, the optimization problem for atomic clusters becomes, essentially, the search for the minimum of the modelling function. This problem, which is very simple for the case of two particles, becomes nontrivial even for non-so-high dimensions since the number of minima of the PES usually increases exponentially with the size of the system. An example of this is the cluster of 55 atoms interacting by a LJ potential, LJ_{55} , for which the number of minima is at least 10^{10} . LJ potential is a widespread binary potential that has been investigated intensively and serves as a good model for inert gas clusters [1].

Given the potential difficult of the problem, the development of effective methods for its resolution is an intensive area of research. In the recent years, different approaches have been proposed for finding the minima of potential energy functions used when modelling clusters and some of them have achieved promising results. One of these approaches, the Basin-Hopping method, has been able to find all the global minima for LJ clusters containing up to 110 atoms through unbiased searches [3]. An unbiased search is a search in which the algorithm does not start with a configuration that is close to that of the global minimum (also called seed). The development of methods that posses great performance even in unbiased searches is fundamental, since these could be applied for more than one problem.

This work aims to serve as an introduction to the global optimization in the context of

atomic clusters. Firstly, a formal proposition for the general global optimization problem (GOP) is given and then a particular case of study is proposed: the search for the global energy minimum for clusters containing up to 50 atoms. For this purpose, two potentials, LJ and M, are introduced and the optimization method commented above, BH [3], is implemented using Python. Also, some analysis on the performance of the algorithm is given.

2 The global optimization problem (GOP) and the methods for its resolution

Resumen

La optimización global es una rama de las matemáticas cuyo objetivo es obtener el máximo o el mínimo absoluto de una función o un conjunto de funciones definidas en un dominio concreto y sujetas -o no- a un conjunto de restricciones. Así, el problema de optimización global (POG) se plantea formalmente y supone, en muchos casos, un reto realmente complicado incluso cuando las funciones a optimizar son de pocas variables. No obstante, este tipo de problemas aparece en una gran cantidad de casos prácticos en múltiples disciplinas, que incluyen desde economía (véase el problema del comercial) hasta microbiología, y donde la consecución del valor óptimo puede resultar en grandes ventajas económicas. De esta forma, la optimización global es un campo de gran interés en la actualidad y en el que es necesario la obtención de métodos fiables y eficaces. Algunos de estos, desarrollados en los últimos años, han logrado buenos resultados aplicados a sistemas como biomoléculas, cristales y agregados atómicos o moleculares [1].

The general GOP

Global optimization is a field of applied mathematics that strives to obtain the absolute maximum or minimum of a function or a group of functions in a defined domain. The global optimization problem (GOP) can be formally stated as follows [4]:

$$\begin{array}{ll} \min & f(\mathbf{x}) \\ \text{subject to} & \{g_j(\mathbf{x}) \leq 0; j = 1, \dots, J\} \end{array}$$

where the notation refers to:

- $\mathbf{x} = (x_1, x_2, \dots, x_n) \in \mathbb{R}^n$: real n-vector of **decision variables**,
- $f : \mathbb{R}^n \rightarrow \mathbb{R}$: continuous **objective function**,
- $\mathbf{g} = (g_1(\mathbf{x}), g_2(\mathbf{x}), \dots, g_J(\mathbf{x})) : \mathbb{R}^n \rightarrow \mathbb{R}^m$: finite collection (J-vector) of continuous **constraint functions**.

Keeping all this in mind one can verify, by the classical theorem of Weierstrass, that the optimal solution set of the GOP is non-empty. This set of globally optimal solutions

can be denoted as X^* .

Solving the GOP theoretically requires the determination of the mentioned set X^* or at least an exact global solution $x^* \in X^*$ and the associated optimal value $f^* = f(x^*)$. However, in practice, this is usually not achievable since global optimization models can be really difficult even in very low dimensions (see Figure 2.1). Also, the available set of methods for (local) numerical optimization does not suffice to handle this problem. The mentioned routines for finding local minima (or maxima) may get caught in one of the -many- valleys of the objective function surface, thus not exploring other available configurations. Despite this difficulties, finding the solution to a GOP plays an important role in many different fields since it has a broad span of practical applications that range from assembly line design to computational modeling of atomic and molecular structures (which will be later illustrated in this work) [5].

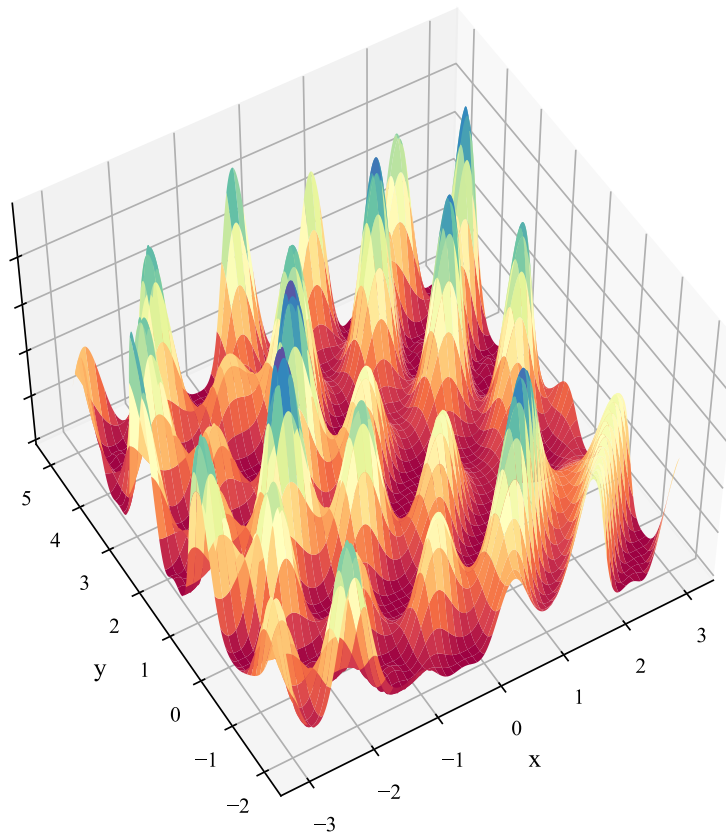


Figure 2.1: Surface plot of the function $f(x, y) = [\sin(xy) + \sin(3y - 5x) + \sin(x^2 - 4y) - 2]^2$ within the domain $D = \{-3 \leq x \leq 3; -2 \leq y \leq 5\}$ to illustrate how complex the GOP can become in higher dimensions and bigger domains.

Global optimization is subject of intense current interest and the development of improved methods for solving GOPs are of great economic importance since the solutions

result in reduced costs or improved performance [1]. A global optimization method consists of an algorithm that can be used for solving one or various GOPs. Even though nowadays there is no general method for solving optimization problems, there are lots of different approaches that obtain great results. Since this work is focused on potential energy functions that describe systems such as atomic clusters, it is relevant to describe some of the strategies that have been found to work best with this type of systems, paying special attention to those that succeed even when no additional information (seed) about the system is given at the beginning. These are the so called unbiased algorithms and play an important role because they can be transferable to other systems.

As an example, simulated annealing probably provided the first generally applicable technique for global optimization [1]. In this method, the state of the system is followed by simulation as the temperature is decreased slowly from a high value. The different possible configurations of the system are obtained through random generation and are then compared. If the new configuration is “*more optimal*”, then it replaces the old one. Otherwise, the new configuration is only accepted if the Metropolis criterion is met. After this process is repeated a given number of times, the temperature is decreased and if no stop condition is fulfilled, then the procedure starts again. On the other hand, a different approach is given by genetic algorithms that mimic the evolutionary process by evolving a “*genetic code*” using the concepts of fitness, mutation and crossover [1]. Finally, other strategy is based on “hypersurface deformation” where the potential energy surface (PES) is deliberately altered. Some techniques related to this approach present an important problem: the global minimum of the altered surface needs to be mapped back to the original surface which in most cases is not easy. Despite these drawbacks, there is a method consisting on hypersurface deformation that has proven its great performance in studies related to atomic and molecular clusters, as well as biomolecules. This approach is known as *basin-hopping* and it is described in the next sections.

The case study: atomic clusters

An atomic cluster is a group of atoms that forms a structure bigger than a simple molecule, but smaller than a nanoparticle. These structures can be modeled by using an adequate potential energy function $V(\mathbf{x})$, where \mathbf{x} is the $3N$ -dimensional vector of nuclear coordinates of the N atoms conforming the cluster. Then, searching the state of minimum energy of the cluster is the same as searching the minimum of the potential energy function, which gives a particular GOP to solve. In this case, there are no constraint functions and the problem is just to find the configuration of the constituents that minimizes the potential energy function. This is, find \mathbf{x}_{min} such that $V(\mathbf{x}_{min}) < V(\mathbf{x})$ where $\mathbf{x} \in \mathbb{R}^{3N}$ and $\mathbf{x} \neq \mathbf{x}_{min}$.

3 Interatomic potentials

Resumen

A la hora de estudiar los agregados atómicos, es esencial disponer de funciones analíticas que den cuenta de la forma más exacta posible de las interacciones entre los átomos constituyentes, pues estas contribuyen a la energía total del sistema. De hecho, para temperaturas cercanas al cero absoluto, esta energía de interacción (o potencial) domina sobre la cinética, pues apenas hay movimiento. A este efecto, existen numerosos potenciales interatómicos. Entre todos ellos, destacan los que se formulan dentro del marco de la aproximación de Born-Oppenheimer, que permite separar los movimientos electrónico y nuclear. Asimismo, los potenciales interatómicos pueden clasificarse atendiendo a si consideran exclusivamente la interacción entre pares de átomos o entre conjuntos más numerosos de estos (tres átomos, cuatro átomos, etc.).

En este trabajo se utilizan dos potenciales bastante extendidos en la literatura científica: el potencial de Lennard-Jones y el potencial de Morse. Ambos consideran únicamente la interacción entre pares de átomos y dependen de las distancias internucleares entre estos. Igualmente, tienen dos contribuciones: un término que da cuenta de las fuerzas de repulsión que aparecen a pequeñas distancias debido al solapamiento de las nubes electrónicas de los átomos y otro término que describe la atracción que existe entre los átomos a distancias mayores debido a la aparición de dipolos inducidos.

When studying atomic clusters it is essential to have a potential energy function that describes well enough the interaction between the constituent atoms. It is then fundamental to have enough accurate potential energy functions for optimization methods to be predictive (as commented in [1]).

The two potentials used in this work, LJ and M, depend only on the internuclear distances between the atoms that make up the clusters. This dependency can be justified taking into account Born-Oppenheimer approximation, which allows to separate electron and atomic nuclei motion when describing a cluster.

The Born-Oppenheimer approximation

Due to its importance, a further look in the Born-Oppenheimer approximation is given [6]. Consider a cluster constituted by n electrons with mass m_e and charge e and N nuclei with mass M_t and charge $Z_t e$ (where Z_t denotes the atomic number). The position vector of a nucleus is denoted as \mathbf{R}_t . Thus, the positions of all the nuclei are given by

$\mathbf{R} = \{\mathbf{R}_t\}_{t=1,\dots,N}$. Equally, the position vectors of the electrons are $\{\mathbf{r}_1, \mathbf{r}_2, \dots, \mathbf{r}_n\} \equiv \{\mathbf{r}_i\}_{i=1,\dots,n} = \mathbf{r}$. On the other hand, the Hamiltonian operator of the system can be expressed as:

$$H = T_N + T_e + V \quad (3.1)$$

where T_N and T_e are the kinetic energy operators for the nuclei and the electrons respectively and V is the total potential energy of the cluster. Each of the terms can be written as follows:

$$\begin{aligned} T_N &= - \sum_{t=1}^N \frac{\hbar^2}{2M_t} \nabla_{\mathbf{R}_t}^2 ; & T_e &= - \sum_{i=1}^n \frac{\hbar^2}{2m_e} \nabla_{\mathbf{r}_i}^2 \\ V(\mathbf{R}; \mathbf{r}) &= \frac{e^2}{4\pi\epsilon_0} \left[- \sum_{i=1}^n \sum_{t=1}^N \frac{Z_t}{|\mathbf{r}_i - \mathbf{R}_t|} + \sum_{i<j=1}^n \frac{1}{|\mathbf{r}_i - \mathbf{r}_j|} + \sum_{s<t=1}^N \frac{Z_s Z_t}{|\mathbf{R}_s - \mathbf{R}_t|} \right] \end{aligned} \quad (3.2)$$

where ϵ_0 is the vacuum permittivity, \hbar is the reduced Planck constant and $\nabla_{\mathbf{R}_t}^2, \nabla_{\mathbf{r}_i}^2$ indicate that the corresponding derivatives are carried out with respect to the coordinates associated with the t -th nucleus and the i -th electron respectively. Also, the potential V , which is given by the Coulomb interaction, has three different contributions: the electron-electron interactions V_{ee} , the electron-nucleus interactions V_{en} and the nucleus-nucleus interactions V_{nn} .

For this system, the time-independent Schrödinger equation may be written as:

$$H\Psi(\mathbf{R}, \mathbf{r}) = E\Psi(\mathbf{R}, \mathbf{r}) \quad (3.3)$$

Due to the presence of the distance terms in the potential it is impossible to obtain an analytical solution by separating the variables. However, an ansatz of the following form is proposed:

$$\Psi(\mathbf{R}, \mathbf{r}) = \psi_{\mathbf{R}}^{(e)}(\mathbf{r})\chi^{(N)}(\mathbf{R}) \quad (3.4)$$

in this expression $\psi_{\mathbf{R}}^{(e)}(\mathbf{r})$ and $\chi^{(N)}(\mathbf{R})$ are the electronic and nuclear wavefunctions respectively. The subindex \mathbf{R} in $\psi_{\mathbf{R}}^{(e)}(\mathbf{r})$ indicates that the function depends parametrically on the coordinates of the nuclei, which means that different electronic wavefunctions are obtained for each configuration of the nuclei. Also, note that $\psi_{\mathbf{R}}^{(e)}(\mathbf{r})$ depends on the coordinates of the electrons \mathbf{r} , while $\chi^{(N)}(\mathbf{R})$ depends on those of the nuclei \mathbf{R} . Now, the proposed solution is introduced in the Schrödinger equation, giving:

$$\begin{aligned}
 H\psi_{\mathbf{R}}^{(e)}(\mathbf{r})\chi^{(N)}(\mathbf{R}) &= \chi^{(N)}(\mathbf{R})T_e\psi_{\mathbf{R}}^{(e)}(\mathbf{r}) + \psi_{\mathbf{R}}^{(e)}(\mathbf{r})T_N\chi^{(N)}(\mathbf{R}) + V\psi_{\mathbf{R}}^{(e)}(\mathbf{r})\chi^{(N)}(\mathbf{R}) - \\
 - \sum_{t=1}^N \frac{\hbar^2}{2M_t} &\left[2\nabla_{\mathbf{R}_t}(\chi^{(N)}(\mathbf{R})) \cdot \nabla_{\mathbf{R}_t}(\psi_{\mathbf{R}}^{(e)}(\mathbf{r})) + \chi^{(N)}(\mathbf{R})\nabla_{\mathbf{R}}^2\psi_{\mathbf{R}}^{(e)}(\mathbf{r}) \right] = E\psi_{\mathbf{R}}^{(e)}(\mathbf{r})\chi^{(N)}(\mathbf{R})
 \end{aligned} \tag{3.5}$$

In this expression the last term is different from zero because the electronic wavefunction $\psi_{\mathbf{R}}^{(e)}(\mathbf{r})$ depends on the nuclear coordinates \mathbf{R} , so the derivatives $\nabla_{\mathbf{R}_t}\psi_{\mathbf{R}}^{(e)}(\mathbf{r})$ and $\nabla_{\mathbf{R}_t}^2\psi_{\mathbf{R}}^{(e)}(\mathbf{r})$ are non-zero. Nevertheless, since the nuclear masses M_t appear in the denominator, it is a reasonable assumption that the last term is small and then can be neglected. This is the Born-Oppenheimer approximation. Taking this into account, the Equation 3.5 can be rewritten as:

$$\psi_{\mathbf{R}}^{(e)}(\mathbf{r})T_N\chi^{(N)}(\mathbf{R}) + \left(T_e\psi_{\mathbf{R}}^{(e)}(\mathbf{r}) + V\psi_{\mathbf{R}}^{(e)}(\mathbf{r}) \right) \chi^{(N)}(\mathbf{R}) = E^{(BO)}\psi_{\mathbf{R}}^{(e)}(\mathbf{r})\chi^{(N)}(\mathbf{R}) \tag{3.6}$$

where $E^{(BO)}$ is the total energy of the cluster estimated within the Born-Oppenheimer approximation. As a first step for solving this equation, the next equality is considered for fixed values of the nuclear coordinates \mathbf{R} :

$$(T_e + V)\psi_{\mathbf{R}}^{(e)}(\mathbf{r}) = E_e(\mathbf{R})\psi_{\mathbf{R}}^{(e)}(\mathbf{r}) \tag{3.7}$$

This is the Schrödinger equation for the so called electronic Hamiltonian and describes the state of the electrons in the potential V that depends on the fixed positions of the nuclei \mathbf{R} . The eigenstate is the electronic wavefunction $\psi_{\mathbf{R}}^{(e)}(\mathbf{r})$ and the eigenvalue $E_e(\mathbf{R})$ is the electronic contribution to the total energy of the molecule plus the potential energy of internuclear repulsion at the fixed nuclear positions. If plotted against the nuclear positions, the eigenvalue gives the potential energy surface (PES). This PES is formed using the ground electronic state, which is the most probable configuration at low temperatures.

Finally, Equation 3.6 can be rewritten as:

$$\begin{aligned}
 \psi_{\mathbf{R}}^{(e)}(\mathbf{r})T_N\chi^{(N)}(\mathbf{R}) + E_e(\mathbf{R})\psi_{\mathbf{R}}^{(e)}(\mathbf{r})\chi^{(N)}(\mathbf{R}) &= E^{(BO)}\psi_{\mathbf{R}}^{(e)}(\mathbf{r})\chi^{(N)}(\mathbf{R}) \Rightarrow \\
 \Rightarrow [T_N + E_e(\mathbf{R})]\chi^{(N)}(\mathbf{R}) &= E^{(BO)}\chi^{(N)}(\mathbf{R})
 \end{aligned} \tag{3.8}$$

which is the Schrödinger equation for the wavefunction of the nuclei $\chi^{(N)}(\mathbf{R})$ when the nuclear potential energy, now $E_e(\mathbf{R})$, has the form of the potential energy surface.

Thus, the Born-Oppenheimer approximation allows to separate nuclear and electronic

motion, as well as to introduce the concept of potential energy surface (PES) which plays an essential role in the studies on the structure of clusters.

Interatomic potentials

Given a system of N atoms, its potential energy V consists on the sum of the energetic interactions between the atoms [7]. This energy V can be formally expanded in a series of terms that depend on the individual atoms, pairs of atoms, groups of three atoms, etc. Thus:

$$V = \sum_{i=1}^N v_1(\mathbf{r}_i) + \sum_{j<i=1}^N v_2(\mathbf{r}_i, \mathbf{r}_j) + \sum_{i=1}^N \sum_{j=1}^N \sum_{k=1}^N{}' v_3(\mathbf{r}_i, \mathbf{r}_j, \mathbf{r}_k) + \dots \quad (3.9)$$

Here the notation $'$ indicates that the $i=j=k$ terms are not included in the summation and \mathbf{r}_i is the position of the i -th atom. The first term is associated to the effect of external forces or boundary conditions. Therefore, if no force is acting on the system (as it is considered in this work), the first summation equals zero. v_2 describes the interaction between the pair of atoms with positions r_i and r_j , ignoring the rest of them and so the second term accounts for the two body interactions; note that the condition $j < i$ is imposed so the pairs are only counted once. The third term describes the so called three-body interactions. If a fourth term were included, it would account for the four-body interactions of atoms and so on.

Regarding the expression given for V in Equation 3.9, and for the purposes of this project, interatomic potentials will be classified in two different groups: pair potentials and many-body potentials. The first ones are constructed taking into account only the second term of Equation 3.9 while the second ones include the description of three-body interactions, four-body interactions and so on. Both the potentials used in this work, LJ and M, are pair potentials.

The Lennard-Jones (LJ) potential

The LJ potential describes the interaction energy of two or more non-bonding atoms. As commented above, it is a pair potential and it depends on the distance between the particles. This potential has demonstrated to provide a useful model for noble gas clusters and, even though there are more accurate models concerning these systems, it is quite widespread due to its computational efficiency. Lennard-Jones potential also provides a helpful testing ground for different global optimization methods [1].

This potential has two contributions: a repulsive term which describes the repulsion of the interacting particles at short distances due to the overlapping of electronic clouds

and an attractive term that accounts for the attractive forces that appear because of the existence of induced dipoles. The functional form of the potential is:

$$V_{LJ}(\{r_{ij}\}) = \sum_{i < j=1}^N 4\epsilon \left[\left(\frac{\sigma}{r_{ij}} \right)^{12} - \left(\frac{\sigma}{r_{ij}} \right)^6 \right] \quad (3.10)$$

where $\{r_{ij}\}$ is the set of distances between the atoms, ϵ is the depth of the potential well and σ is the distance at which the potential between two particles is zero. Note that this two parameters depend on the pair of atoms that are interacting and therefore this form of the LJ potential is only valid for systems of N equal atoms. For all the purposes of this work, reduced units were used and so $\epsilon, \sigma = 1$.

In the expression (3.10) the repulsive (first) and the attractive (second) terms can be identified. It can be seen that for distances $r_{ij} < \sigma$ the repulsive term is more important than the attractive one and that the opposite happens when $r_{ij} > \sigma$. Also, both terms tend to zero when $r_{ij} \rightarrow \infty$. Therefore, three different situations are possible: the atoms of the system are so far away from each other that they are not interacting, they are just in the range of distances where they tend to come closer or they are so close that they are repelling each other.

The simplest situation is given by a system of 2 particles. In this case, the potential only depends on one variable -the inter-particle distance r - and it is easy to obtain its global minimum which is found to be $V_{LJ} = -1$ with the distance r being $2^{1/6}$. This case is shown in the Figure 3.1.

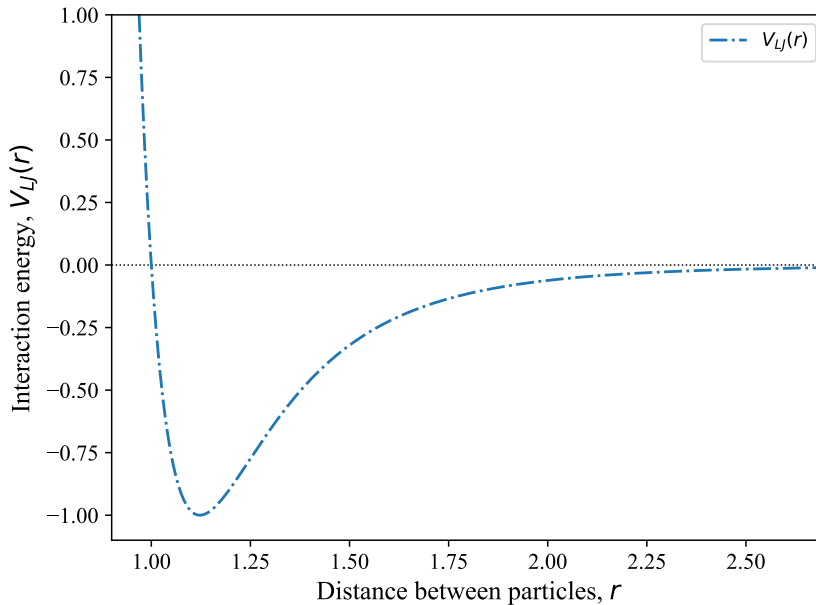


Figure 3.1: LJ potential for a 2 particle system.

The Morse (M) potential

When studying the interaction forces between atoms in a molecule, a widely used model due to its mathematical advantages is the harmonic oscillator model. However, real molecular vibrations are anharmonic so other potentials must be proposed in order to achieve new models that are more accurate. Amongst many molecular potentials, M potential (proposed by Morse in the year 1929) is an anharmonic potential which allows an exact mathematical treatment [8]. Also, as the LJ potential, M potential has two contributions: one term associated to the repulsive forces that appear at short distances and another term which describes the forces of attraction that are present at bigger distances.

The M potential may be written in different forms. The expression used in this work for a system of N equal atoms is [9]:

$$V_M(\{r_{ij}\}) = \epsilon \sum_{i < j=1}^N e^{\rho_0(1-r_{ij}/r_0)} (e^{\rho_0(1-r_{ij}/r_0)} - 2) \quad (3.11)$$

as for the LJ potential, $\{r_{ij}\}$ is the set of distances between the atoms and ϵ is the depth of the potential well. Also, r_0 is the equilibrium pair separation -note that for the two particle case $V_M = -1$ when $r_{12} = r_0$ - and ρ_0 is an adjustable parameter that determines the range of the interparticle forces. If ρ_0 is decreased, then the range of the attractive part increases and the repulsive wall becomes less steep, thus widening the potential well. If ρ_0 is increased, the result is the opposite. This can be seen in Figure 3.2.

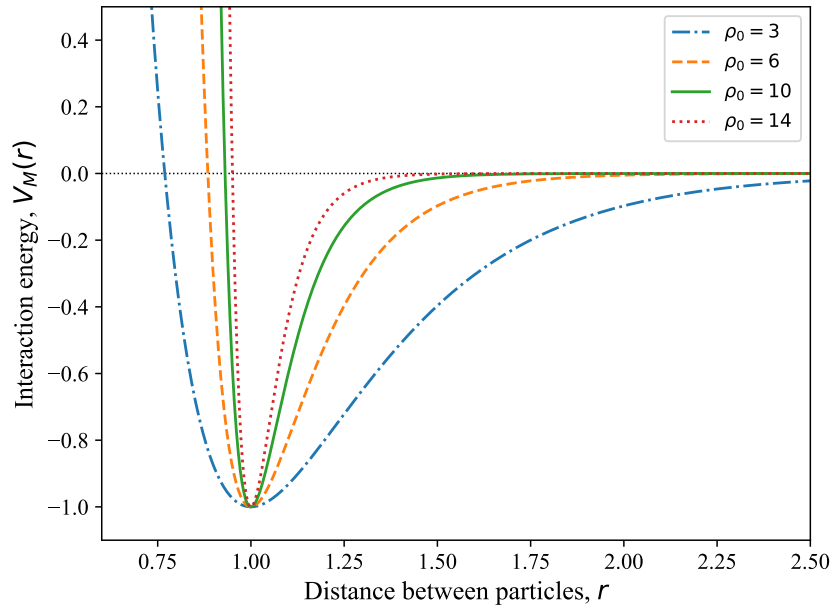


Figure 3.2: M potential for different values of the variable parameter ρ_0 .

Due to the parameter ρ_0 , the M potential can be used for studying different systems, as opposite to the LJ potential, which was accurate for describing rare gases structures only. Indeed, some research is focused on studying how the range of the interaction affects the energy minimum for a system with a given number N of particles, and also how changing N affects the geometry for a given range. It has been found that the parameter ρ_0 determines the favored structures of atomic clusters. According to the bibliography [10], four main structural regimes were found for M clusters. For very long-ranged interaction potentials, the structures are highly strained, highly coordinated, spherical and not based on any regular package. For large sizes these structures show little order and have similarities to the liquid-like structures characteristic of shorter ranges. At intermediate ranges of the potential, icosahedral structures are dominant. As the range decreases from short to very short, first decahedral and then fcc structures dominate (see Figure 3.3). Decreasing the range of the potential and increasing the size of the cluster have similar effects on strained structures: both actions destabilize these. As an example, the lowest-energy structures of LJ clusters change from icosahedral to decahedral to fcc as the size increases. For M clusters this change in the geometry is also expected to depend on the range of the potential.

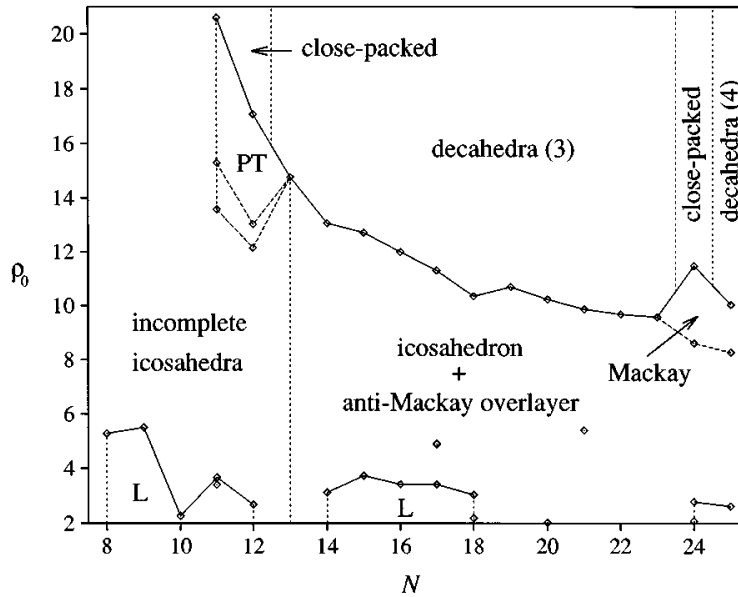


Figure 3.3: “Phase diagram” showing how lowest-energy structures change according to the values of N and ρ_0 . PT means polytetrahedral structures and L structures associated with low ρ_0 . Extracted from [10].

However, in this work, only one value of ρ_0 was used. For $\rho_0 = 6$ the M potential has the same curvature at the bottom of the well as the LJ potential [8] (this can be seen in Figure 3.4). With this knowledge, a comparison between the curves of the two potential energy functions is carried on. For this purpose, still using reduced units $\epsilon, \sigma = 1$, the

equilibrium pair separation r_0 of the Morse potential is set to $2^{1/6}$ so the minimum of both curves concur.

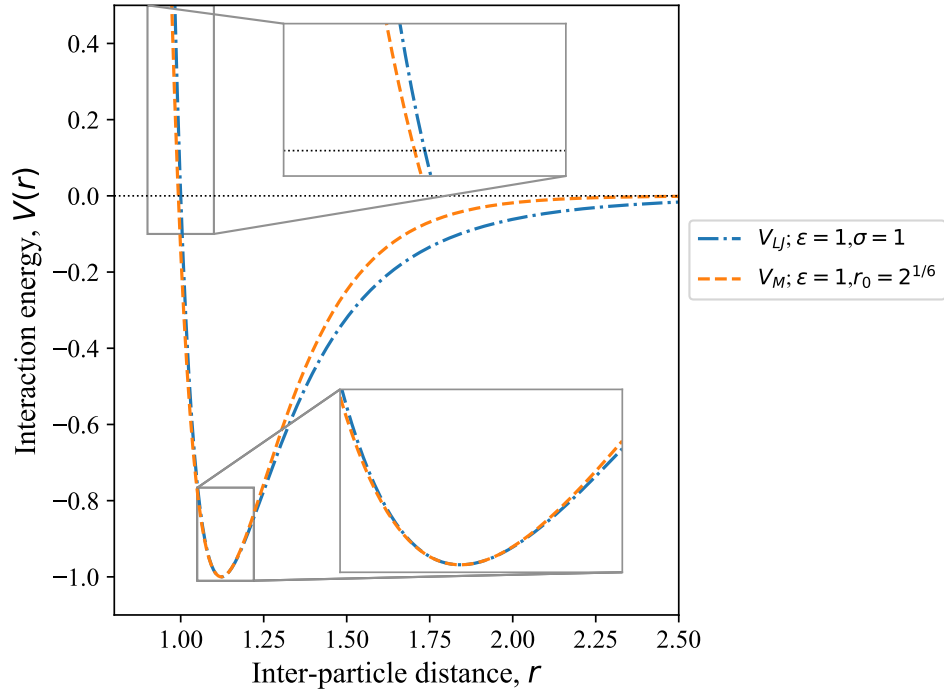


Figure 3.4: A representation of both the M and the LJ potentials.

Despite the curvature of the potentials being the same at the bottom of the well, in Figure 3.4 it is noticeable that M potential has a less steep repulsive part and that the width of its well associated to the attractive forces is smaller than that of the LJ potential. This means that if the system is being modelled using the M potential with $\rho_0 = 6$, the range of the interaction forces will be slightly smaller than if the LJ potential was used.

4 The implemented method: Basin-Hopping

Resumen

Con el algoritmo implementado, que se ha extraído directamente de un artículo de Wales y Doye [3], se explora la hipersuperficie de energía potencial de los agregados atómicos utilizando una simulación de Monte Carlo. Esto se combina con una rutina de minimización local (en este caso se ha escogido el método del gradiente conjugado) para obtener diferentes configuraciones del sistema en las que la energía potencial es mínima. En cada iteración se obtiene un valor de la energía, $V_{min}^{(new)}$, que se compara con el valor obtenido en una iteración anterior $V_{min}^{(old)}$. Si $V_{min}^{(new)} < V_{min}^{(old)}$, entonces se acepta el salto y el estado pasa a ser $V_{min}^{(new)}$. Si $V_{min}^{(new)} > V_{min}^{(old)}$, solo se acepta el salto si se cumple el criterio de Metrópolis y, en caso de aceptarse, también se redefine $V_{min}^{(old)} = V_{min}^{(new)}$ (es decir, que el estado pasa a ser $V_{min}^{(new)}$). Si no se cumple ninguna de las dos condiciones anteriores, el salto no se acepta y en la siguiente iteración se vuelve a perturbar desde la misma configuración. En este caso, se estudia el sistema a una temperatura T fija y finita. El proceso de perturbación y minimización se repite hasta que se alcance una condición de parada. Para el algoritmo desarrollado se ejecutaba un número fijado de iteraciones y luego se detenía. Asimismo, las energías más pequeñas encontradas se van archivando, de tal forma que se obtiene una lista de energías en orden decreciente.

Además de las mejoras de rendimiento que conciernen al desarrollo del código, el método basin-hopping muestra un desempeño u otro en base a los valores de temperatura T y paso d . Cada problema a resolver, esto es, cada agregado a estudiar, presenta valores óptimos concretos para T y d . Sin embargo, encontrar dicha pareja de valores es una tarea que conlleva mucho tiempo. Es por esto -y porque los casos estudiados son problemas ya resueltos-, que los valores de T y d se han fijado de acuerdo a los indicados en el trabajo original de Wales y Doye [3].

The fundamentals of the algorithm

First of all, it is important to introduce the concept of catchment basin. A catchment basin is a region in which the function is convex (also called a valley). All optimisation methods which combine search techniques and catchment basin transformation are known as basin-hopping methods [1]. In this type of hypersurface transformations the potential energy of every point in a catchment basin becomes the energy of the minimum of the basin. Thus, the original potential energy surface (PES), that may have any morphology, is mapped onto a stairlike surface in which each plateau is associated

to a minimum of the original PES. This strategy allows to search for the global minimum using hypersurface deformation without affecting the values of the original minima.

This work is focused on applying an unbiased basin-hopping optimization routine to different potential energy functions used for modeling atomic clusters. The method implemented is extracted from an article by Wales and Doye [3] and it is programmed using Python. In this basin-hopping approach, the potential energy surface is explored using a canonical Monte Carlo simulation at a fixed reduced temperature (see Figure 4.1 for a flowchart of the algorithm).

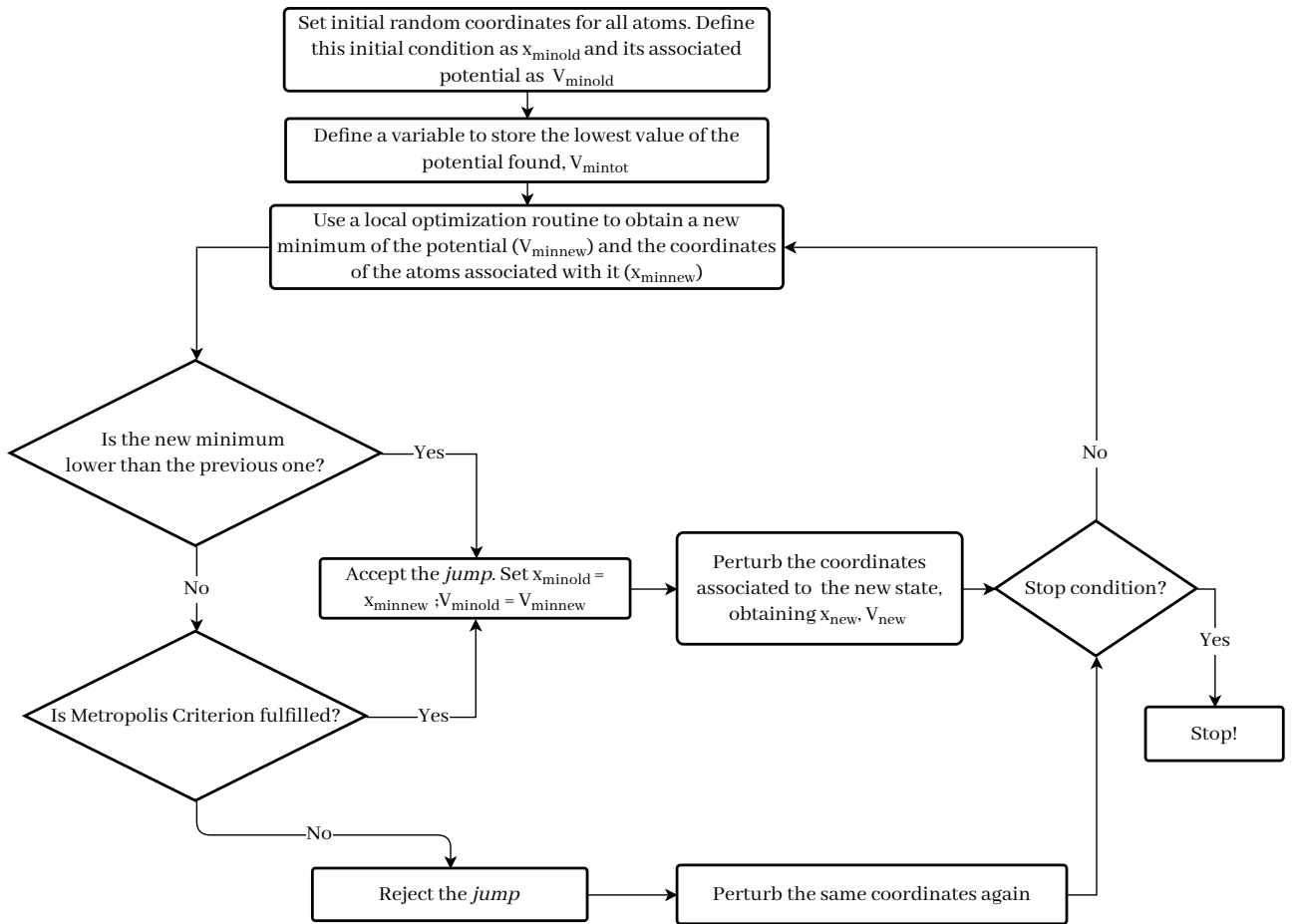


Figure 4.1: Flowchart for the BH method.

Initially, a random configuration of the system is generated. It is given by \boldsymbol{x}_0 , the $3N$ -dimensional vector of nuclear coordinates. An easy way of achieving this is to place the N atoms on the surface of a sphere of given radius. This initial state has an potential energy associated which is defined as V_0 . Also, a variable that will store the lowest value of the potential energy found, $V_{\min}^{(\text{tot})}$, is defined at this point. This can be done by

giving it the value of V_0 or just any other high value so it will be replaced after the first minimization. Once all variables are defined, a local minimization routine is carried on. The result obtained through this is a new configuration, $\mathbf{x}_{min}^{(old)}$, that has a lower value for the potential energy, $V_{min}^{(old)}$, than the random generated state with V_0 . This is the procedure followed for PES deformation and can be expressed as:

$$\tilde{E}(\mathbf{x}) = \min\{E(\mathbf{x})\} \quad (4.1)$$

where \mathbf{x} is the 3N-dimensional vector of nuclear coordinates and \min denotes that the energy minimization is performed starting from \mathbf{x} [3]. Also, since initially $V_{min}^{(tot)}$ was defined as an arbitrary high value, it is always replaced by the value of $V_{min}^{(old)}$ in the first iteration.

After the new configuration is obtained, a random perturbation is performed on it. For each component of $\mathbf{x}_{min}^{(old)}$, the perturbation can be written as:

$$(\mathbf{x}_{new})_i = (\mathbf{x}_{min}^{(old)})_i + 2d(\xi_i - 0.5) \quad (4.2)$$

where \mathbf{x}_{new} is the vector of the new state, d is the biggest distance that an atom can be displaced in each direction and ξ_i is an uniformly distributed random number in the interval (0,1).

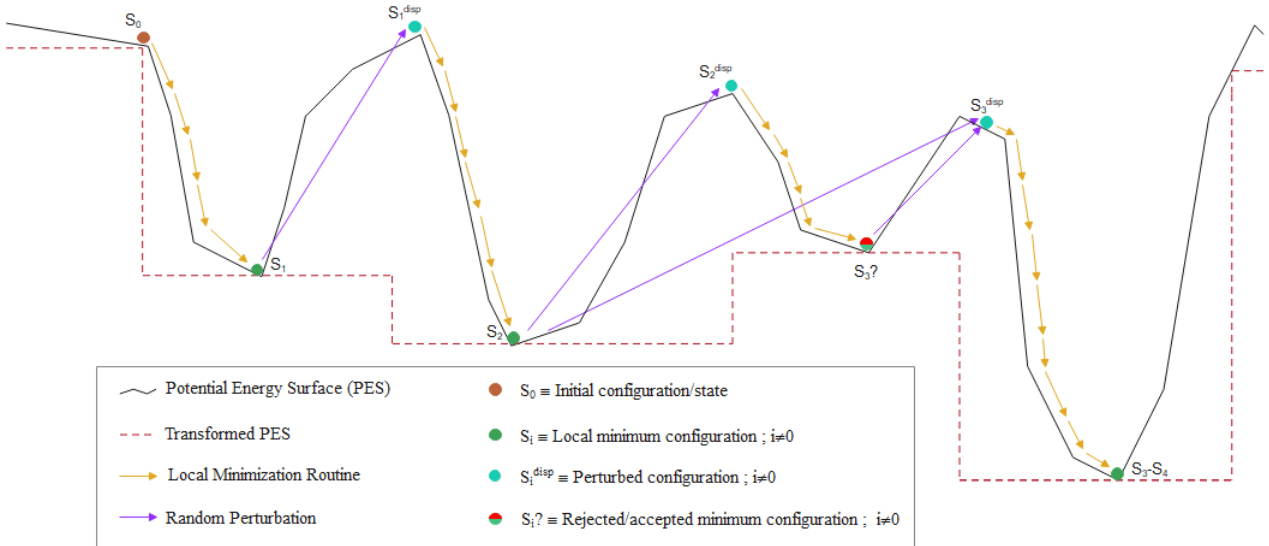


Figure 4.2: Scheme of the functioning of the BH method in a simple one dimensional case.

After the perturbation is applied, the process of local minimization is repeated. As a result, $\mathbf{x}_{min}^{(new)}$ and $V_{min}^{(new)}$ are obtained. Now there are two different situations:

- 1) $V_{min}^{(new)} < V_{min}^{(old)}$. The perturbation is accepted and $V_{min}^{(new)}$ becomes the new state (so the following redefinitions are done: $V_{min}^{(old)} = V_{min}^{(new)}$, $\mathbf{x}_{min}^{(old)} = \mathbf{x}_{min}^{(new)}$). Additionally, if $V_{min}^{(new)} < V_{min}^{(tot)}$, then $V_{min}^{(tot)} = V_{min}^{(new)}$ and the value of the new minimum is saved (note that this is always true for the first iteration, as commented above).
- 2) $V_{min}^{(new)} > V_{min}^{(old)}$. In this case, the perturbation is only accepted if:

$$e^{(V_{min}^{(old)} - V_{min}^{(new)})/k_B T} > \zeta \quad (4.3)$$

where k_B is the Boltzmann constant -with value 1 in reduced units-, T is the temperature of the system (which is fixed at some finite reduced value) and ζ is an uniformly distributed random number in the interval (0,1). This condition is known as Metropolis criterion and prevents the method from getting stuck in one minimum, thus allowing it to explore more of the configuration space. As before, if the criterion is met and the perturbation is accepted, then $V_{min}^{(new)}$ becomes the new state (and so $V_{min}^{(old)} = V_{min}^{(new)}$, $\mathbf{x}_{min}^{(old)} = \mathbf{x}_{min}^{(new)}$). On the other hand, if the Metropolis Criterion is not fulfilled, in the next iteration the algorithm applies a new random perturbation to \mathbf{x}_{old} again. Also, in this case, even if the perturbation was accepted, it would be senseless to compare $V_{min}^{(new)}$ with $V_{min}^{(tot)}$, since in all the cases $V_{min}^{(new)} > V_{min}^{(tot)}$.

These procedures are repeated in each iteration until a stop condition is met. Since generally in global optimization the optimal value of the objective function is unknown, two options are considered for the stop condition:

1. **Stop condition based on the precision achieved.** If after a given number of iterations the best result obtained for the global minimum does not improve significantly, then the algorithm stops.
2. **Stop condition based on the number of iterations.** In this case, the criterion is just to run a number given of iterations. For example, if the number of iterations is fixed at 1000, the algorithm will stop when 1000 iterations are performed. This is the condition used in this work.

Algorithm and code efficiency

As commented in the previous sections, the general GOP is rather a difficult problem. Due to this, it is expectable that the different methods implemented for solving optimization problems require a lot of computational cost. It is then interesting to optimize the code developed (redundant as it sounds) as much as possible in order to make the calculations less time-consuming. However, apart from code specificities, there are

two parameters in the Basin-Hopping method that can be changed to achieve a better performance. These are: the temperature T and the maximum perturbation size or step d . The local minimization routine can also be changed and improved for a better performance, but in the case of this project an already existing Python function for the conjugate gradient method was used. Note that for implementing this local search routine, the analytical expressions of the gradients of the potential functions are needed. They are given in the appendices.

The values of the temperature T and the perturbation size d are related to the acceptance of new solutions in each iteration. In the case of the temperature, it is directly related to the Metropolis criterion. According to Equation 4.3, lower values of T lead to a higher probability of accepting new solutions while the bigger values diminish it. On the other hand, the value of the parameter d determines how much of the configuration space is *explored*. High values of the step lead to more energetic states that are more unlikely to be accepted while low values give “*solid-like*” states which have greater probabilities of being accepted. Thus, if the step d is too small, the algorithm could easily get trapped in a local minimum, but if it is too big, the method may not explore the surroundings of a minimum near to the global and fail to find this. In both situations, the absolute minimum is missed, so this parameter must be well chosen for the method to succeed. An option to approach this issue is to define a variable step that changes according to the value of the acceptance rate, which is given by the quotient between the solutions accepted and the iterations performed. For example, if the objective acceptance rate is 50%, the variable step could be set such that after a given number of iterations this rate is evaluated. If the value obtained is smaller than 0.5, then the step is decreased so states with lesser energy are obtained. On the other side, if the acceptance rate is greater than 0.5, then the step is increased so solutions that are more likely to be rejected are achieved. Both conditions aim to maintain the acceptance rate around the desired value.

In spite of all of the commented above, the optimal values of the temperature and the step varies from one cluster to another and finding these is a rather time-consuming task. It must be taken into account that the algorithm may fail to find the global minimum in some of the runs (which is unlikely for many of the smallest clusters) and that, in order to compare the performance with different pairs (T, d) , the executions need to be repeated -and be succesful- a considerably amount of times. Due to all this, and since this project is focused on checking that the unbiased basin-hopping method achieves to find the global minima for all the clusters up to 50 atoms rather than improving the performance for already solved problems, the temperature and the step were fixed at $T = 0.8$, $d = 0.3$, which are the values mentioned in the original work of Wales and Doye [3].

5 Results and analysis

Resumen

Utilizando el método BH se han obtenido las energías mínimas para los agregados de hasta 50 átomos modelizados tanto por el potencial LJ como el M. Los resultados obtenidos se han comparado con los valores disponibles en la base de datos de Cambridge [11][12]. Con estos resultados, se observa que los agregados de LJ tienen menor energía que los de M y que la diferencia de energía entre ambos se va acentuando conforme aumenta el número de átomos. También se concluye que, como se esperaba, el agregado que mayor dificultad ha planteado de cara a la obtención del mínimo de energía ha sido el de 38 átomos.

Por otro lado, a la hora de estudiar agregados atómicos, un parámetro muy utilizado está dado por las segundas diferencias en las energías, que dan cuenta de la estabilidad relativa de los distintos agregados. Este parámetro se ha calculado para cada uno de los agregados estudiados, concluyendo que las estructuras más estables se encuentran para $N = 13, 19, 23, 26, 29, 32, 36, 39, 43, 46$ y 49 . Estos números se conocen como “numeros mágicos”, ya que son aquellos para los que los agregados son especialmente estables. Se han representado las estructuras de los clústeres para esos valores de N y se observa que estas se basan en empaquetamiento icosaédrico, tal y como se menciona en la bibliografía [3]. Adicionalmente, se han representado las dos estructuras de menor energía para el agregado de 38 átomos. En este caso, el mínimo global no presenta empaquetamiento icosaédrico, sino que conforma el denominado octaedro truncado. Sin embargo, la estructura que presenta el segundo valor más pequeño de la energía sí se basa en empaquetamiento icosaédrico.

The results for the energies

The basin-hopping algorithm implemented in this work has found all the lowest known minima up to LJ_{50} and M_{50} . The results obtained were compared with the values available in The Cambridge Energy Landscape Database [11][12]. The energy per particle obtained for each cluster of N atoms is represented in Figure 5.1.

The energies for M and LJ clusters are different for clusters with more than four atoms due to the different shapes of both potentials. Only for $N = 2, 3, 4$ the distance between atoms corresponds to the equilibrium pair distance $2^{1/6}$. For clusters with more atoms, it is not possible to place all of them simultaneously at that distance and so the ground-state energy increase. In Figure 5.1 it is noticeable that the difference between

the energies of the LJ and Morse clusters becomes bigger as the number of atoms of the cluster increases. This is due to the presence of more terms in the potentials. A further insight of this increment is given in Figure 5.2. However, despite the energies obtained for the clusters differ depending on which potential is used for describing them, the geometries of their structures are fundamentally the same.

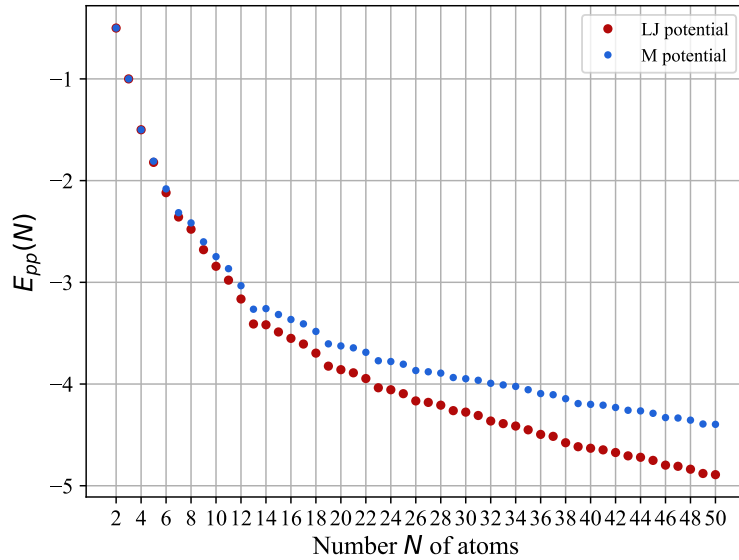


Figure 5.1: Energy per particle obtained for each cluster using LJ and Morse potentials.

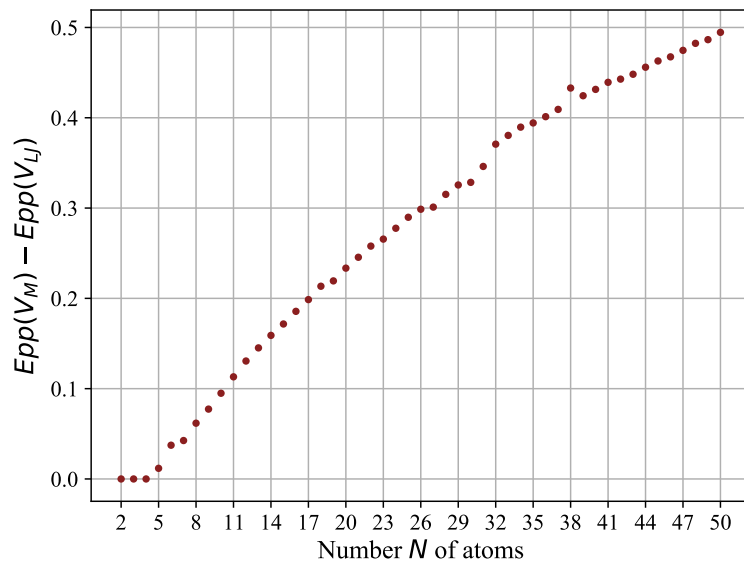


Figure 5.2: Differences between the energies per particle obtained for each cluster with the LJ and M potentials.

These results were obtained with the BH method using 1000 steps in each run, except for the aggregate with $N = 38$, for which 5000 steps were employed due to its high difficulty. As commented in the previous section, the step d was fixed at 0.3 and the temperature at $T = 0.8$. Five different trajectories were done for each cluster. A rather important value for characterizing the difficulty of each cluster is the number of solutions/jumps accepted until its global minimum is reached. Using the data of the five trajectories for each cluster, in Figure 5.3 the mean number of necessary jumps for achieving the global minimum is represented against the number of atoms N .

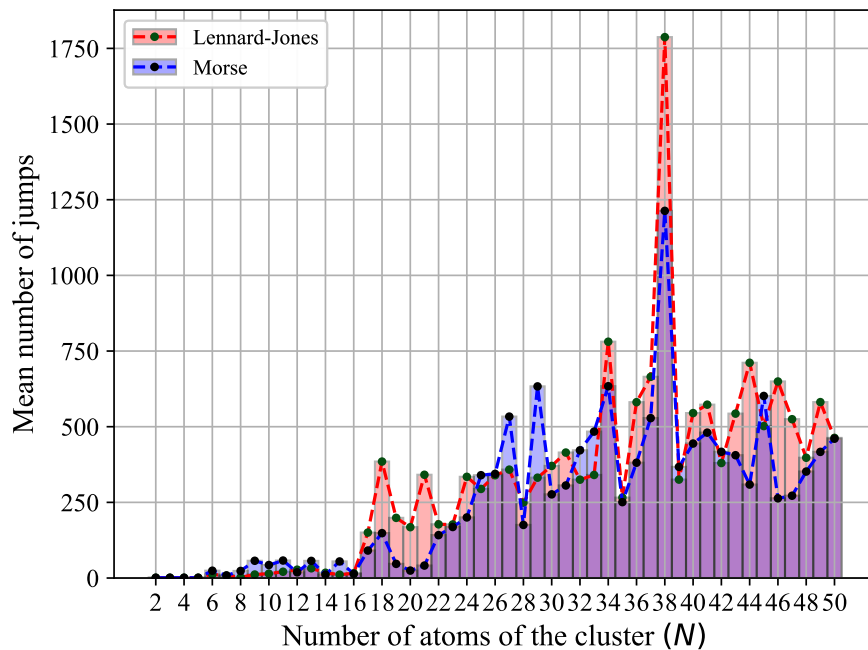


Figure 5.3: Representation of the mean number of necessary jumps for achieving the global minimum for each of the clusters size.

As expected, for both potentials, the structure for which more jumps are needed is the cluster with 38 atoms. In this case, the lowest energy minimum based on icosahedral packing acts as a trap and is widely separated from the true global minimum [1] making its search more difficult. Finally, in views of the results obtained, it appears that the M clusters are easier to optimize than the LJ clusters. However, it is not possible to assert this since the number of studied trajectories is very low, so the results have no statistical significance.

Cluster stability and geometry

As commented above, even though the energies of the clusters are different depending on which potential is being used, the structures found for both of them are essentially

the same. Taking this into account, the following discussion is centered exclusively on the LJ clusters.

According to the bibliography, most global minima for LJ clusters containing less than 100 atoms are based on icosahedral packing [1]. The results obtained with the basin-hopping algorithm implemented allowed to check this fact in clusters containing up to 50 atoms as well as to study the structure of one of the exceptions, LJ_{38} . The stability of the different structures obtained is discussed taking into account the second-order difference of cluster energies.

Second-order difference of cluster energies

The second-order difference of cluster energies, denoted as $\Delta_2 E(N)$, is a widespread physical parameter that reflects the relative stability of the clusters [13]. It is given by the equation:

$$\Delta_2 E(N) = E(N + 1) + E(N - 1) - 2E(N) \quad (5.1)$$

Given this definition, the set of more stable structures among all the obtained is given by those which have a greater value of $\Delta_2 E(N)$. In Figure 5.4 the value of the second-order energy difference is represented for each cluster.

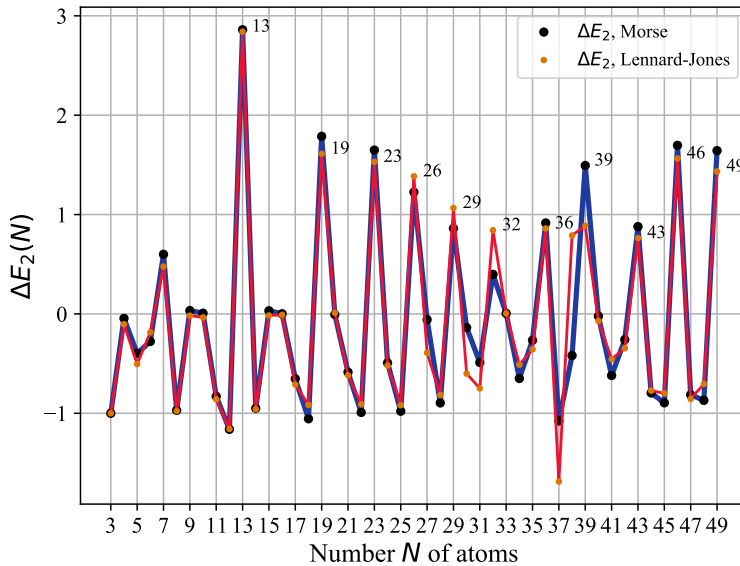


Figure 5.4: A representation of the second-order energy differences $\Delta_2 E(N)$ for each cluster size and both potentials, LJ and M.

According to this figure, the more stable clusters are found for $N = 13, 19, 23, 26, 29, 32, 36, 39, 43, 46$ and 49 . Some studies have shown that some of these structures ($N = 13, 19, 23, 26$) appear when decreasing the temperature of an initial gas state of particles

interacting with a LJ potential [14]. A common name given to the numbers for which the stability is especially high is *magic numbers*. The more relevant cases are those of $N = 13$ and $N = 19$. But, what is the geometry of the so found structures?

Geometry of the clusters

It has already been commented that the most common structures for LJ clusters are based on icosahedral packing. A regular icosahedron is a polyhedron with 20 faces, being each of them an equilateral triangle. Moreover, many small clusters are polytetrahedral in the sense that the whole of the cluster can be divided into tetrahedra. Also, many clusters are made up of different layers of close-packed atoms. Both categories include the cluster LJ_{13} , which forms a complete Mackay icosahedron and can be decomposed in twenty tetrahedra sharing a common vertex.

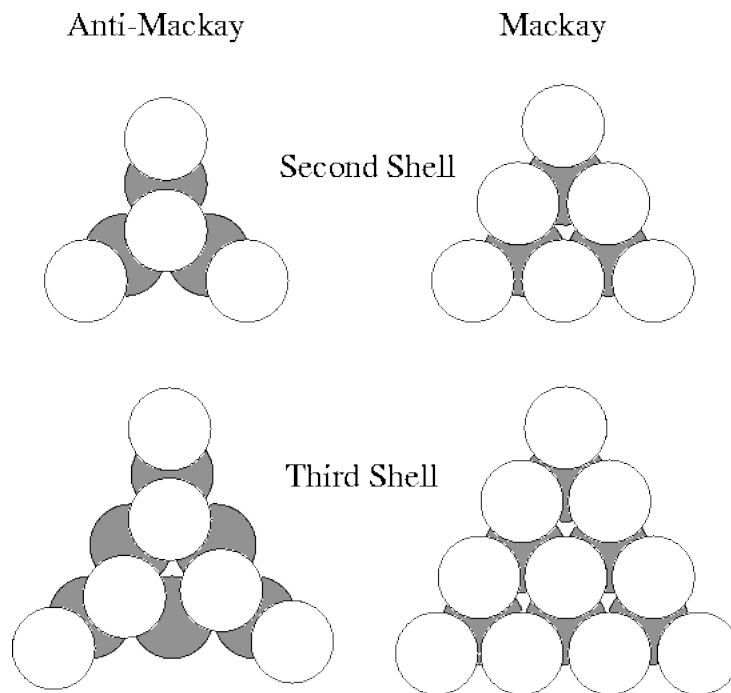


Figure 5.5: Atomic positions for the two possible overlayers of the icosahedron, anti-Mackay (left) and Mackay (right). These are shown for a single face of the icosahedron. Extracted from [15].

The addition of atoms to the icosahedron can occur in two different ways and the types of resulting overlayers are shown in Figure 5.5. The first growth mode (fcc-like) continues the fcc packing present in the 13-atom cluster and leads to the 55-atom Mackay icosahedron. The second growth mode, *anti-Mackay*, involves sites that are hexagonal-close-packed (hcp) with respect to the tetrahedra and so the resulting structure is not an icosahedron. Therefore, the close-packing of one structure varies according to the growth mode. Finally, for LJ clusters, when the number of atoms does not allow to

form a complete Mackay icosahedron, the resulting structure can be described in terms of a Mackay icosahedron in the “core” with a shell/layer of some type (Mackay/anti-Mackay)[15].

Icosahedral structures

The structures obtained for the clusters whose second-order difference energy is higher are represented in Figure 5.6. Cluster LJ_{13} is the one with greater stability according with Figure 5.4 and this is reaffirmed by the fact that it forms a complete Mackay icosahedron. Additionally, in Figure 5.1 it can be seen that the LJ_{13} cluster has almost the same energy per particle as the LJ_{14} , which accounts for the remarkable stability of the 13-atom cluster. Similarly, in the case of the M potential, M_{13} has less energy per particle than M_{14} .

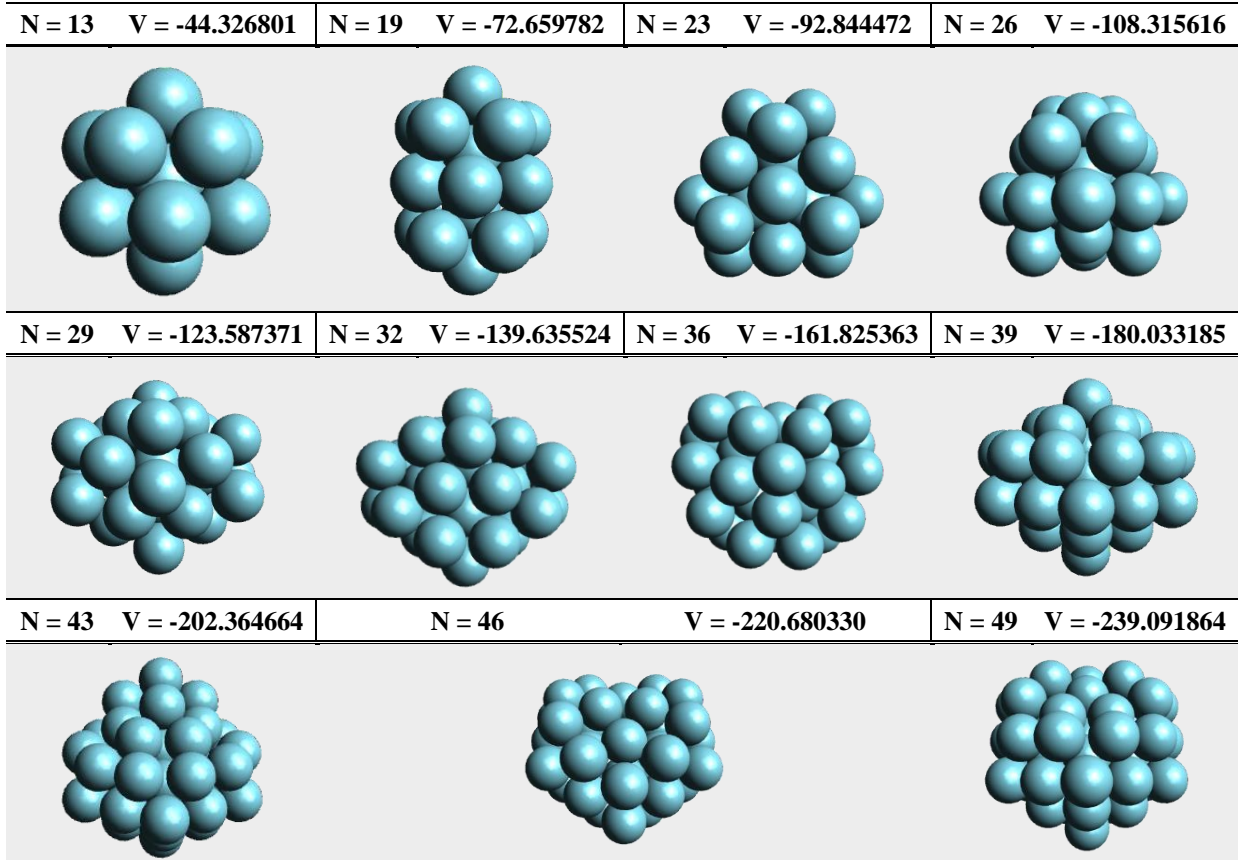


Figure 5.6: Structures obtained for the so called “magic numbers”, clusters with a certain number of atoms which give rise to a particularly high stability.

On the other hand, the other peaks corresponding to $N = 19, 23$ and 26 are associated to a double, triple and quadruple icosahedron, which are formed by growth of an anti-Mackay overlayer. This overlayer is completed at 45 atoms, giving as a result a structure called rhombic triacontahedron, which can be described as an icosahedron

of interpenetrating icosahedra [16]. However, note that the 45-atom cluster does not present a high stability (see Figure 5.4).

The 38-atom cluster

The case for $N = 38$ was the most difficult case studied. As seen in Figure 5.3, the number of steps required for the BH method to succeed in the search for the global minimum for $N = 38$ is, by far, the higher one among all the cases studied -being higher for the case of the LJ potential-.

As commented above, for the search for the minimum of LJ_{38} five trajectories of 5000 steps were performed. The number of steps accepted until reaching this minimum in each trajectory is given in Table 5.1.

Trajectory	Number of steps
1	3819
2	599
3	1906
4	230
5	2382

Table 5.1: Results obtained in each trajectory for the cluster LJ_{38} using the BH method implemented.

In addition to the trajectories in which the global minimum was located, other trajectories were performed in which the second lowest energy structure was found. Its energy is -173.252478 , very close to that of the global minimum. In the case of the 38-atom cluster, this configuration compete in the search with the one of the global minimum due to the complicated form of the PES. This fact can be portrayed in a disconnectivity graph. A disconnectivity graph is a tree that shows the number of basins present at a discrete set of energies [17]. Its branching structure shows how the basins at one energy level are related to those at successive lower energies. At high enough energies, all the minima are contained in one basin (or superbasin, since other basins are contained in it) and the end of the branches correspond to the energies of the minima.

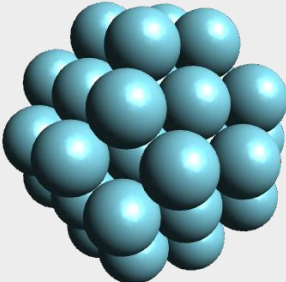
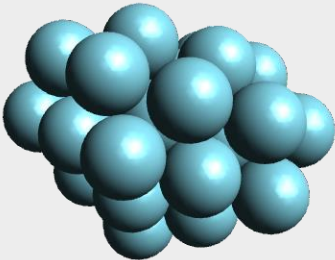
N = 38	
Truncated octahedron	Incomplete Mackay icosahedron
V = -173.928427	V = -173.252378
	

Figure 5.7: The global minimum structure (left) and the second lowest energy structures (right) found for the LJ_{38} cluster.

The study of the 38-atom cluster case is very interesting because the most stable structure is not based on icosahedral packing and due to the PES form the GOP poses a greater difficulty than for other clusters studied. In the $N = 38$ case, the lowest energy structure is a face-centered-cubic (fcc) truncated octahedron. A regular octahedron is a polyhedron with eight faces, being all of them equilateral triangles. Albeit this structure is not based on icosahedral packing, the structure associated to the second lowest energy do have icosahedral structure. A comparison between the structures of the global minimum and the second lowest energy structure is given in Figure 5.7.

6 Conclusions

Resumen

El método basin-hopping implementado en este proyecto se plantea como una herramienta bastante capaz a la hora de encontrar los mínimos globales de distintos agregados atómicos, pues ha sido capaz de encontrar estos para los agregados de LJ y de M de hasta 50 átomos partiendo de una configuración aleatoria.

Igualmente, como se comentaba en la bibliografía [3], la eficiencia del método implementado puede mejorarse de diferentes formas: a través de un estudio más detallado de los parámetros de la temperatura T y el paso d , a través de la combinación de este método con otros que también han probado su eficiencia o bien mediante la introducción de semillas, es decir, haciendo que el algoritmo empiece desde una estructura con una geometría concreta y no con una configuración aleatoria.

Finalmente, en este trabajo no ha podido estimarse cuál de los dos potenciales utilizados plantea una mayor complejidad. Sin embargo, un estudio más exhaustivo en el que se realizasen más trayectorias para los correspondientes agregados, permitiría llevar a cabo dicha comparación.

The method implemented in this work has been capable of locating all of the global minimum energies for the LJ and M clusters containing up to 50 atoms through unbiased searches. This agrees with the results from previous works of the bibliography [3].

The most complex system studied has been the 38-atom cluster, which agrees with what is said in the bibliography [1]. In this case, more steps, 5000 instead of 1000, were required. Taking this into account, it is to be expected that the method implemented would fail to obtain the global minimum for other difficult clusters such as LJ_{75-77} if the number of steps is fixed at 5000. A possible solution to this is to increase the number of steps performed before the search routine is stopped, since the more time is expended searching for a minimum along a specific trajectory, the more probable it is to find it. Another possible improvement is given by changing T and d according to if not enough solutions are being accepted or if, on the opposite, too much are being accepted. Also, other approach could be to introduce the variable step that was commented in the section destined to the BH method and a variable temperature which varies according to the acceptance rate too. Other possibilities for improving the efficiency of the algorithm are mentioned on [3] and include combining the implemented BH method with other global optimization techniques or seeding the algorithm instead of starting from random

configurations.

Finally, as commented above, in the results obtained for both LJ and M potential it appears that the LJ clusters are more complicated to optimize than the M clusters. Nevertheless, since the number of trajectories performed is very low to carry on a statistical treatment, the results are not conclusive. A more exhaustive study where more trajectories were performed for both type of cluster would be enough for giving a reasonable comparison between the difficulty they pose.

References

- [1] David J. Wales and Harold A. Scheraga. “Global Optimization of Clusters, Crystals, and Biomolecules”. In: *Science* 285 (1999), pp. 1368–1372.
- [2] Encyclopaedia Britannica. *Cluster*. 2019. URL: <https://www.britannica.com/print/article/122615> (visited on 07/01/2021).
- [3] David J. Wales and Jonathan P.K. Doye. “Global Optimization by Basin-Hopping and the Lowest Energy Structures of Lennard-Jones Cluster Containing up to 110 Atoms”. In: *J.Phys.Chem.A* 101 (1997), pp. 5111–5116.
- [4] Panos M. Pardalos and H. Edwin Romeijn. *Handbook of Global Optimization*. Kluwer, 2002.
- [5] Panos M. Pardalos. *Global Optimization: Scientific and Engineering Case Studies*. Springer, 2006.
- [6] Peter Atkins and Ronald Friedman. *Molecular Quantum Mechanics*. Oxford University Press, 2005.
- [7] Richard Lesar. *Introduction to Computational Materials Science: Fundamentals to Applications*. Cambridge University Press, 2013.
- [8] Shi-Hai Dong. *Factorization Method in Quantum Mechanics*. Springer, 2007.
- [9] John Doye. *Morse Potential*. 1997. URL: <http://doye.chem.ox.ac.uk/jon/structures/Morse/potential.html> (visited on 06/04/2021).
- [10] J. P. K. Doye, D. J. Wales, and R. S. Berry. “The effect of the range of the potential on the structures of clusters”. In: *The Journal of chemical physics* 103.10 (1995), pp. 4234–4249.
- [11] David J. Wales et al. *Table of Lennard-Jones Cluster Minima*. URL: <http://doye.chem.ox.ac.uk/jon/structures/LJ/tables.150.html> (visited on 06/29/2021).
- [12] D. J. Wales et al. *Morse Clusters Table*. URL: <http://doye.chem.ox.ac.uk/jon/structures/Morse/tables.html> (visited on 06/29/2021).
- [13] Xiao-Juan Feng and You-Hua Luo. “Structure and Stability of Al-Doped Boron Clusters by the Density-Functional Theory”. In: *The Journal of Physical Chemistry A* 111.12 (2007), pp. 2420–2425.
- [14] Ikeshoji Tamio, Hafskjold Bjorn, Hashi Yuichi, et al. “Molecular Dynamics Simulation for the Formation of Magic-Number Clusters with a Lennard-Jones Potential”. In: *Physical Review Letters* 76 (1996), pp. 1792–1795.
- [15] D. J. Wales et al. *Icosahedral clusters*. 1997. URL: <http://doye.chem.ox.ac.uk/jon/structures/Morse/paper/node6.html> (visited on 06/30/2021).
- [16] David J. Wales. *Energy Landscapes With Applications to Clusters, Biomolecules and Glasses*. Cambridge University Press, 2003.

REFERENCES

- [17] Elaine Angelino. *Disconnectivity graphs*. 2013. URL: <https://lips.cs.princeton.edu/disconnectivity-graphs/> (visited on 07/01/2021).

Appendix A: Derivatives of the Lennard-Jones and Morse potentials.

Lennard-Jones

$$\frac{dV_{LJ}(\mathbf{r})}{dr_{kj}} = -4\epsilon \sum_{j \neq k} (12\sigma^{12}r_{kj}^{-13} - 6\sigma^6r_{kj}^{-7}) \quad (\text{A.1})$$

Morse

$$\frac{dV_M(\mathbf{r})}{dr_{kj}} = \frac{2\rho_0}{r_0}\epsilon \sum_{j \neq k} e^{\rho_0(1-\frac{r_{kj}}{r_0})} \left(1 - e^{\rho_0(1-\frac{r_{kj}}{r_0})}\right) \quad (\text{A.2})$$

Graphic representation in the simple case of two particles

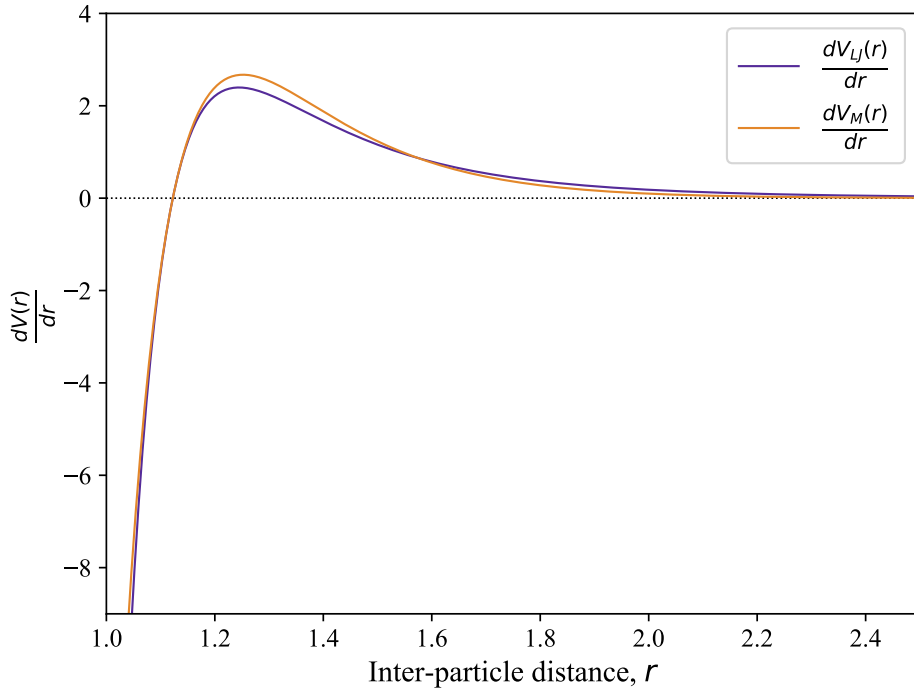
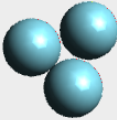
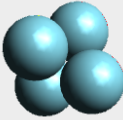

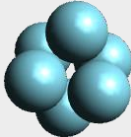
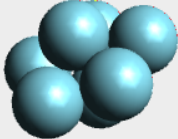
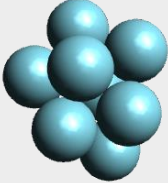
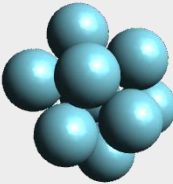
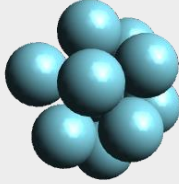
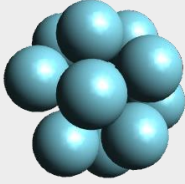
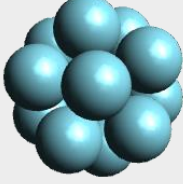
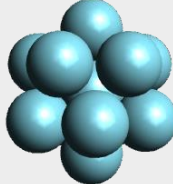
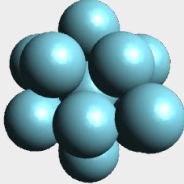
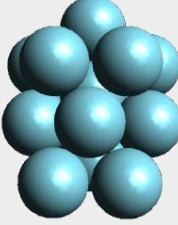
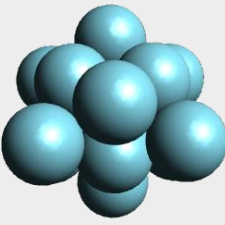
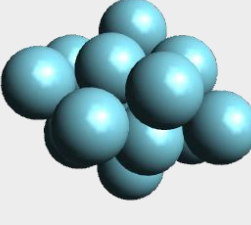
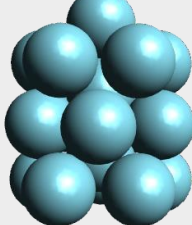
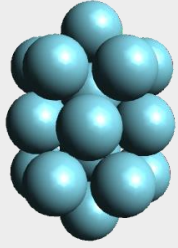
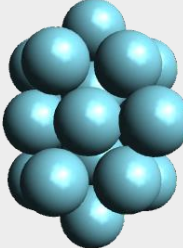
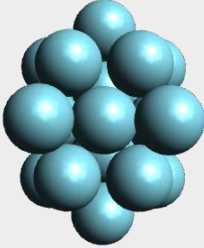
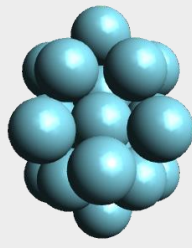
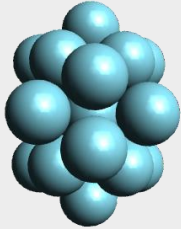
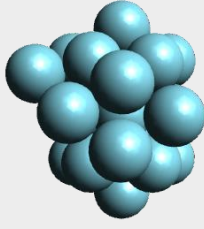
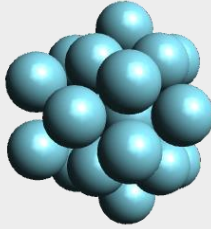
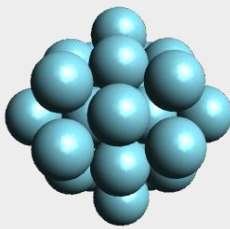
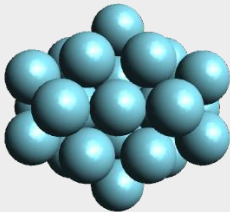
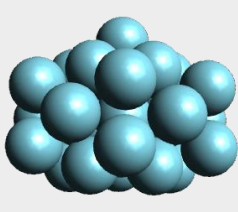
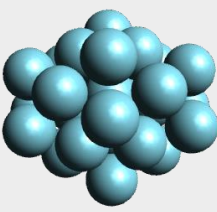
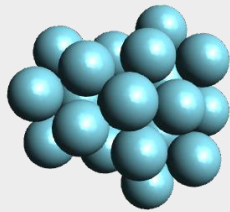
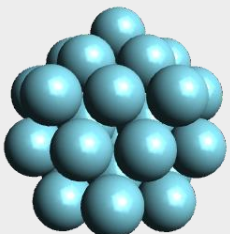
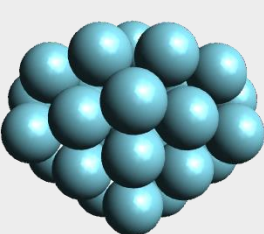
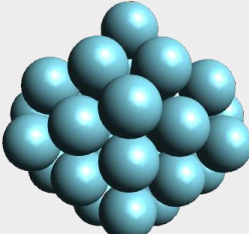
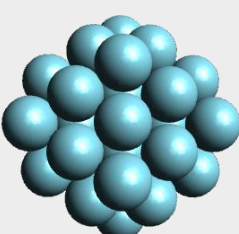
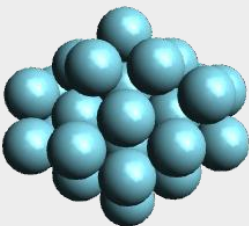
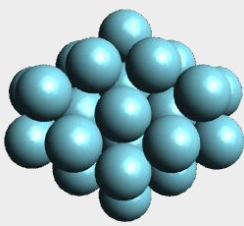
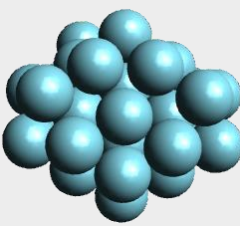
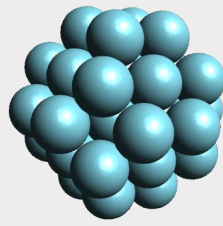
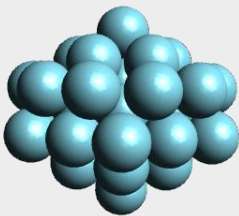
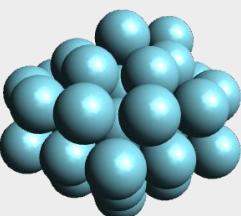
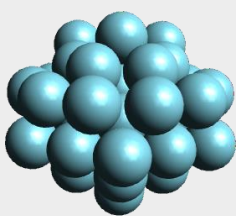
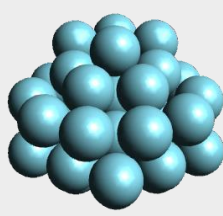


Figure A1: Representation of the derivatives of both potentials, LJ and M, for a two particle system.

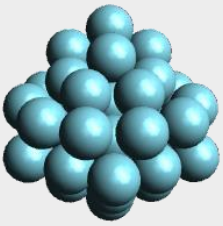
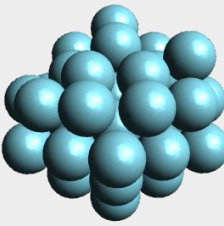
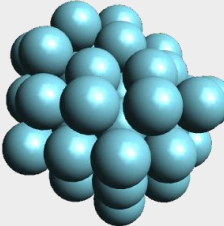
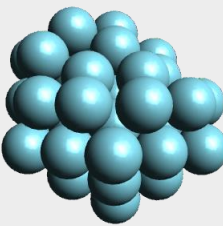
Appendix B: All the structures obtained for the Lennard-Jones potential excluding the 2 particle case.

N = 3 V = -3.000000	N = 4 V = -6.000000	N = 5 V = -9.103852	N = 6 V = -12.712062
			
N = 7 V = -16.505384	N = 8 V = -19.821489	N = 9 V = -24.113360	N = 10 V = -28.422532
			
N = 11 V = -32.765970	N = 12 V = -37.967600	N = 13 V = -44.326801	N = 14 V = -47.845157
			
N = 15 V = -52.322627	N = 16 V = -56.815742	N = 17 V = -61.317995	N = 18 V = -66.530949
			
N = 19 V = -72.659782	N = 20 V = -77.177043	N = 21 V = -81.684571	N = 22 V = -86.809782
			

APPENDIX B: ALL THE STRUCTURES OBTAINED FOR THE LENNARD-JONES POTENTIAL EXCLUDING THE 2 PARTICLE CASE.

N = 23 V = -92.844472	N = 24 V = -97.348815	N = 25 V = -102.372663	N = 26 V = -108.315616
			
N = 27 V = -112.873584	N = 28 V = -117.822402	N = 29 V = -123.587371	N = 30 V = -128.286571
			
N = 31 V = -133.586422	N = 32 V = -139.635524	N = 33 V = -144.842719	N = 34 V = -150.044528
			
N = 35 V = -155.756643	N = 36 V = -161.825363	N = 37 V = -167.033672	N = 38 V = -173.928427
			
N = 39 V = -180.033185	N = 40 V = -185.249839	N = 41 V = -190.536277	N = 42 V = -196.277534
			

APPENDIX B: ALL THE STRUCTURES OBTAINED FOR THE LENNARD-JONES POTENTIAL EXCLUDING THE 2 PARTICLE CASE.

N = 43	V = -202.364664	N = 44	V = -207.688728	N = 45	V = -213.784862	N = 46	V = -220.680330
							
N = 47	V = -226.012256	N = 48	V = -232.199529	N = 49	V = -239.091864	N = 50	V = -244.549926
